Menghua Lu[1]

Lijuan Zhang[1, *]

Jiayi Li[1]

Jie Lu[1]

Fengjiao Liu[1]

Jos J. Derksen[2]

Experiments and simulations of hollow cylinders falling through quiescent liquids

Abstract

We perform quantitative visualization experiments of hollow cylinders falling through Newtonian liquid. The Archimedes number is in the range 5 to 10^5, the length over outer diameter of the cylinders is in the range 2.5 to 10, and the inner over outer diameter is from 0 to 0.85. Our definition of the Archimedes number includes the inner and outer cylinder diameter and we show that cylinders with the same Archimedes number having different diameter ratio behave similarly. Particle-resolved simulations have been used to enhance our insight in the fluid flow generated by the settling cylinder. They also have been used to assess the flow through a hollow cylinder during settling.

Keywords

sedimentation, non-spherical particles, quantitative visualization, particle-resolved simulation

[1]School of Chemistry and Chemical Engineering, Shanghai University of Engineering Science, 333 Longteng Road, Songjiang District, Shanghai, China.

[2] School of Engineering, University of Aberdeen, Regent walk, Aberdeen AB24 3FX United Kingdom.

*Correspondence: Prof. Lijuan Zhang(zhanglj0128@126.com), School of Chemistry and Chemical Engineering, Shanghai University of Engineering Science, 333 Longteng Road, Songjiang District, 201600, Shanghai, China.

1 Introduction

We study sedimentation of a rigid, hollow, cylindrical particle through liquid. There are a number of reasons to study a relatively simple system as this one is. Some reasons directly relate to practical applications, mostly in chemical engineering. Other reasons relate to the development and improvement of modeling of the dynamical behavior of non-spherical particles in fluids with such modeling having practical importance over a broad range of technological applications.

In various branches of engineering, one encounters solid particles suspended in a fluid. In civil and environmental engineering one can think of dredging [1], sediment transport in rivers and coastal areas [2] and waste water treatment. In chemical engineering fluidization and catalytic slurry reactors are used for (reactive) mass transfer between solids and fluid. An application in petroleum engineering is transport of drilling mud (drilling fluid laden with rock cuttings). In modeling such systems and processes, the shape of the solids is often not explicitly considered and particles are – implicitly – assumed spherical. For example, two-fluid models as part of multiphase computational fluid dynamics solvers use correlations for drag on spherical particles to account for fluid-solids interaction [3]. Where the assumption of spherical shape is a very reasonable one for e.g. sand grains and FCC (fluid catalytic cracking) powders, there are situations in which particles deviate so strongly from the spherical form that their shape significantly influences their individual and collective behavior. The processing of biomass is a prominent example [4]. Biomass is a dense suspension containing fibrous solid material that is notoriously difficult to transport and convert [5]. Particles of cylindrical shape are also contained in the thick slurries from which Li-ion battery electrodes are produced [6]. Hollow (cylindrical) particles have the potential for transfer enhancement as a result of the additional surface area of their pore(s). Specific particle shapes have been designed that optimize mass and heat transfer processes in fixed and fluidized bed reactors [7-9].

Particularly for sedimentation, the shape of particles is a decisive factor of how sedimentation processes evolve. In 1969, Strinham et al. [10] studied the settling behavior of the disks, cylinders, oblate and prolate spheroids, and spheres falling in a quiescent liquid, including the particle's orientation, settling speed, and the path traveled. It was concluded that the stability of falling particles is related to the stability of the pressure distribution in the wake of the particle. Komar et al. [11] investigated the influence of particle shape on drag coefficient and settling speed. They used ellipsoidal pebbles falling through glycerol. They interpreted their results in terms of a sphericity shape factor that allows for the estimations of drag coefficients of non-spherical grains. More recently, the motion of freely falling cylinders in a low-viscosity fluid was experimentally studied by Toupoint et al. [12]. The influence of the

Archimedes number (ranging from 200 to 1100) and the length-over-diameter aspect ratio (2 to 20) on the settlement path of the cylinder was reported.

In the research described in this paper we report on experiments of hollow cylinders settling in a Newtonian liquid. Through quantitative visualization we measure how their settling speed and orientation evolve over time starting from vertical release. The effects of the length over outer diameter aspect ratio as well as the outer over inner diameter ratio of the cylinders have been investigated. By varying the size of the cylinders and also the liquid viscosity, we have been able to cover a wide range of Archimedes numbers.

The experiments are supported by numerical simulations that explicitly account for the hollow cylinder shape. One aim of the experiments reported in this paper is to establish a database that can be used for validating simulation work and we want to show here what such validation could look like. Also, the simulations provide additional insights, such as the structure of the liquid flow field induced by the sedimenting particle and the strength of the flow through the cylinder's inner diameter. As discussed above, the latter has potential relevance for applications involving mass transfer. Vice versa, the experimental results are used to assess the quality of the predictions made by the simulations and thus to validate the – inevitable – assumptions and approximations made in designing and executing the simulation procedure.

Our numerical simulations attempt to resolve the flow around – and through – the settling hollow cylinders, i.e. they represent the shape of the particle by solving the flow on a mesh that is finer by one order of magnitude than the outer diameter of the cylinder and explicitly apply no-slip at the solid surfaces. Such particle-resolved simulations (PRS's) are a relatively recent development [13], initially used for flow around moving spheres [14]. PRS's of sedimenting non-spherical particles have been reported by Wachs et al [15]; PRS's of fluidization of cylindrical particles by Derksen [16].

This paper builds upon our previous experimental and numerical work on the settling of solid cylinders [17] where it was shown that the Archimedes number was the principal parameter that determines the sedimentation process, both in terms of settling speed and the evolution of the cylinder's orientation. The current paper extends this work by adding the inner diameter as an additional degree of freedom. By a careful choice of the definition of the Archimedes number for hollow cylinders we are able to have a common framework for settling of solid and hollow cylinders.

This paper is organized along the following lines. The next three sections present the experimental methods and dimensional analysis as well as numerical methods. In the latter section we define the dimensionless numbers that govern the flow system – most importantly the Archimedes number – and discuss the ranges over which they have been varied. In the subsequent Results section, we first show

visualizations of cylinder settling and impressions of the simulations. We quantify the visualizations in terms of cylinder orientation angle and settling speed. Experiments and simulations are compared on those quantities and the way they depend on the Archimedes number and on the cylinder aspect ratios. The final section summarizes, reiterates the main conclusions, and looks forward at future work.

2 Experimental setup

The settling column has a square 80 mm × 80 mm footprint and is 800 mm high. It has transparent (acrylic) side walls. It is filled with a glycerol-water mixture. This is a clear, Newtonian liquid. The relative amount of the two components determines the viscosity and density of the mixture. The temperature of the system was maintained at 25 ± 1 □.

A total of 36 cylindrical particles were utilized in the experiment, most of them hollow. They are all made of stainless steel ($\rho_s = 8.04 g/cm^3$). They have lengths ranging from $l = 1.00$ to 29.20 mm, outer diameters ranging from $d_o = 1.00$ to 2.99 mm, and inner diameter ranging from $d_i = 0$ (solid cylinder) to 1.70 mm. The mass of each cylinder is measured with an electronic balance with an accuracy of ±0.01 mg. The measurement error of cylinder diameter and length is 0.05 mm.

At the start of an experiment, the cylindrical particle was completely immersed in the liquid before being released, ensuring that the hollow space of the cylinder was completely filled with the glycerol-water mixture. Tweezers were used to hold one end of the vertically oriented cylinder while it was slowly lowered into the liquid near the centre of the cross-section of the settling column. When the liquid surface was free of ripples, the tweezers were loosened and the particle was let go with the cylinder vertical within an angle of $\pm 0.5°$.

The settling of the cylinder was filmed with a digital camera. It has 1920 × 1080 pixels and can be operated with variable frame rate f . The frame rate of the camera was adjusted according to the settling speed. Given the frame rate, the position of the centre of gravity of the cylinder can be determined as a function of time. Each pixel represents a square with side length $\delta = 0.77 \pm 0.01$ mm in the liquid column. The particle diameter is less than 4% of the lateral length of the settling column so that – at least during the initial vertical stage of settling – the effect of the walls is small. When the cylinder starts changing its orientation there are occasions when it comes close to, or even touches, one of the side walls. If one end of the cylinder gets in contact with a side wall, that experiment is discarded.

3 Dimensional analysis

In order to generalize the conditions and results obtained in this study, they will be specified and presented mostly in dimensionless form. The hollow cylinders have three length scales: outer diameter d_o, inner diameter d_i and length l, so that there are two independents for which we take l/d_o and d_i/d_o. The solid over liquid density ratio is $\gamma = \rho_s / \rho_l$. The Archimedes number expresses the relative effects of gravity and viscosity in the sedimentation process. For a particle with a single length scale, e.g. a sphere with diameter d, a common definition of the Archimedes number is $Ar = (\gamma - 1) d^3 g / \nu^2$ with g gravitational acceleration and ν the kinematic viscosity. Under highly viscous (i.e. Stokes flow) conditions the sphere's settling velocity is proportional to $(\gamma - 1) d^2 g / \nu$ so that the Archimedes number can be interpreted as a Reynolds number. For the hollow cylinders we have adopted the following definition of the Archimedes number: $Ar = (\gamma - 1)(d_o^2 - d_i^2) d_o g / \nu^2$ with the reasoning that the velocity of a horizontally settling hollow cylinder is proportional to $(\gamma - 1)(d_o^2 - d_i^2) g / \nu$ (the length l to a fair approximation cancels given that drag and net gravity are both proportional to l). If we take d_o as the length scale in the Reynolds number (and thus Archimedes number) we arrive at the above expression for Ar.

If a cylinder – at least a solid one – is vertically released in a Newtonian fluid it will eventually change its orientation to horizontal [17]. The time scales over which this happens and if it happens in a monotonic or a wobbling way depend on the Archimedes number and the aspect ratio(s) [12]. As in our previous paper [17], we characterize this process by measuring two dimensionless parameters. The first is the dimensionless time t_m after which the cylinder reaches a horizontal orientation (i.e. $\theta = 0$) for the first time: $t_m = t_h \nu / d_o^2$ with t_h the dimensional, measured time (in seconds), the relative uncertainty of t_h for repeated experiments is about 5.6%. The second is the Reynolds number at the moment $t = t_h$: $Re = |U| d_o / \nu$, with $|U|$ the absolute value of the vertical velocity of the centre of the cylinder at that moment.

In order to determine $|U|$, we need to analyze the image frames close to the moment the cylinder gets horizontal for the first time. We select two image frames, one before (frame $\#n$) and one after ($\#m$) the moment at which $\theta = 0$ with $2 \le |m - n| \le 5$ and determine the vertical distance traveled by the cylinder's centre of mass δs Then $|U| = \delta s / \delta t$ with $\delta t = |m - n| / f$ and f the frame rate. The uncertainty in δs mainly comes from the size of the pixels, and is estimated to be 1-2 pixels. This leads to a worst-case relative error in $|U|$ of approximately 10%.

Each experiment is repeated at least three times and the values reported (dimensionless velocities and times-to-horizontal) are the averages of the multiple realizations. The error bars presented are the standard deviations of the averages.

4 Simulations setup

We have performed three-dimensional, time-dependent, particle-resolved simulations to compare with the experimental data and to enhance our understanding of the fluid flow phenomena associated with the settling hollow of cylinders. As in our previous paper on settling cylinders [17], the lattice-Boltzmann (LB) method has been used for solving the fluid flow. In the LB method, the flow variables are represented by velocity distribution functions that satisfy a discrete version of the Boltzmann equation [18, 19]. This equation is solved numerically on a cubic lattice with spacing Δ and evolved in time with a time step Δt. The velocity distributions are defined in the center point ("node") of each cubic cell and from the distributions one derives fluid velocity and pressure [20].

At the surface of the (hollow) cylinder, a no-slip condition is imposed through an immersed boundary (IB) method [21]. For this, the surface is defined by a set of closely spaced points (nearest neighbor spacing $\sim 0.5\Delta$). These off-lattice points we call marker points. At each marker point the fluid velocity is determined based on tri-linear interpolation from the lattice nodes and then compared with the solid velocity at that marker point which is known given the linear and angular velocity of the cylinder and the location of the marker point relative to the center location of the cylinder. If the two velocities (of fluid and solid) are different, a force is exerted on the fluid that drives this velocity difference to zero thereby achieving no-slip [22].

Integrating the force distribution over the surface of the cylinder gives the overall force and torque exerted by the fluid on the cylinder. These are used to update the cylinder's linear and angular velocity. We use a split-derivative algorithm to integrate Newton's 2nd law (linear motion) and Euler's equations (rotation) in time with a time step Δt that is the same as the LB time step. Finally, the location and orientation of the cylinder are updated. For the latter a quaternion [23] has been used.

The default spatial resolution of the simulations is such that the outer cylinder diameter spans 12 lattice spacings: $d_o / \Delta = 12$. In previous work [17] it was shown that simulations with higher resolution ($d_o / \Delta = 16$) under the same physical conditions closely matched the ones with the lower resolution of 12. Also, in the current paper such comparisons have been made to establish the effect of spatial resolution for hollow cylinders. The default time step is such that $\Delta t = 7.7 \times 10^{-4} \sqrt{d_o / g}$.

The simulation domain is periodic in all three coordinate directions. This is because it is computationally not feasible to simulate the entire experimental column (also see the discussion on this topic in [17]). The default domain size in the three Cartesian coordinate directions is $nx \cdot ny \cdot nz = 12.5d_o \cdot 5d_o \cdot 150d_o$. With gravity acting in the negative *z*-direction ($\boldsymbol{g} = -g\boldsymbol{e}_z$) we need a tall domain to properly capture the wake behind the cylinder. The hollow cylinder is released fully submerged in still liquid oriented with an angle that deviates 0.5° from fully vertically and with zero velocity; we do this to mimic the angle uncertainty at release in the experiment. The initial slight inclination angle means that – if the cylinder rotates – it will do so around the *y*-axis so that the domain size in *y*-direction can be made relatively small which is helpful for limiting computational time. In our previous work on solid cylinders [17] we have shown that the release angle has only limited effect on the settling process of the cylinder.

5 Results

5.1 The flipping process

In Figure 1 we show impressions of the way the settling process of the cylinders has been visualized, and subsequently analyzed. Time equal zero corresponds to the moment the cylinder was released with vertical orientation. Over time the cylinder rotates to – eventually – achieve a horizontal orientation. At the relatively low Archimedes number ($Ar = 4.95$) in Figure 1 the horizontal orientation is reached monotonically, i.e. the cylinder does not wobble. The camera frames have been analyzed such as to determine the vertical (*z*) of the end points of the cylinder. The vertical distance between the end points Δz, along with the length of the cylinder l allow for determination of the angle θ between the cylinder and the horizontal plane: $\theta = \arcsin(\Delta z / l)$. A time series of θ is shown in Figure 1b.

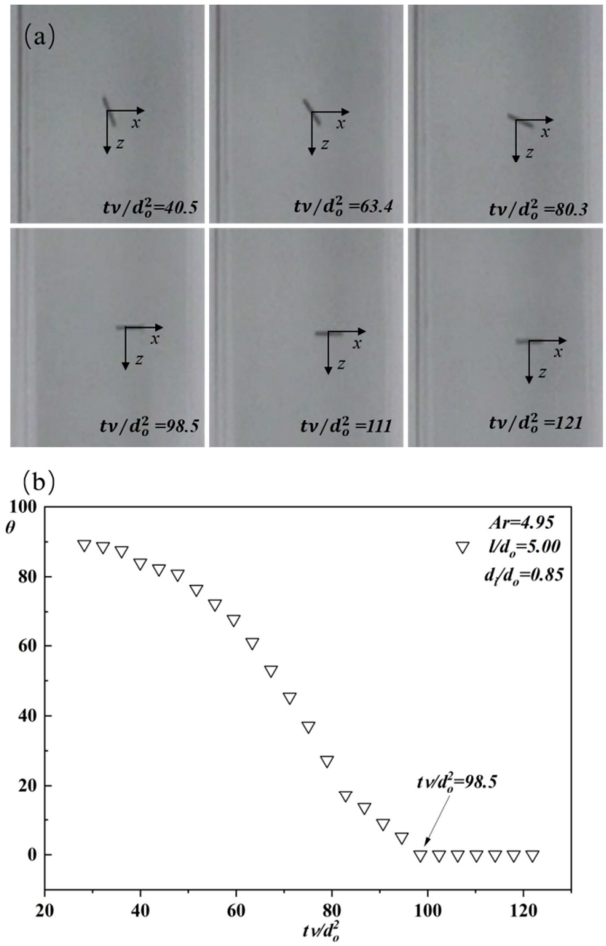

Figure 1. (a) Sample camera frames of a settling experiment recorded at 100 Fps for a $d_i / d_o = 0.85$ and $l / d_o = 5.00$ hollow cylinder falling through a glycerol-water mixture ($Ar = 4.95$). (b) Time series of the angle θ of the hollow cylinder with the horizontal plane.

At higher Archimedes numbers the flipping-to-horizontal is much faster when measured in dimensionless time (tv / d_o^2) and ceases to be monotonic. In Figure 2 we have the same hollow cylinder as used in Figure 1 but now it is falling through less viscous liquids (*m2* and *m9* – see Table S1 of the Supporting Information) and thus at higher Ar . When reaching $\theta = 0$ for the first time the cylinder now continues its rotation and enters a wobbling state. The duration of this state (as measured as the number of wobble periods) and the amplitude of wobbling both increase with increasing Archimedes number (compare the left and the right part of Figure 2).

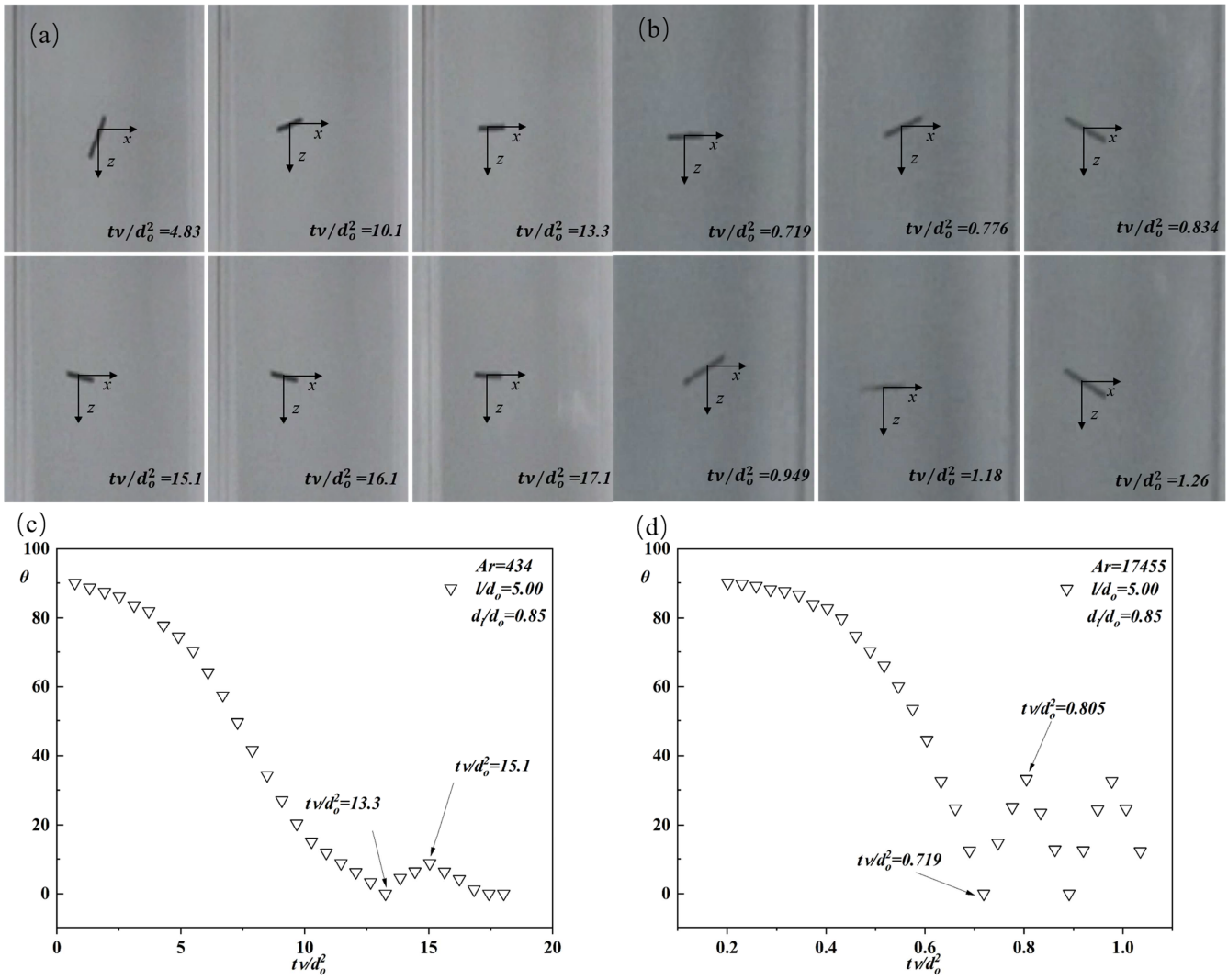

Figure 2. Impressions of the flipping process and the way it depends on Ar. Image frames and corresponding θ time series. (a) and (c) have $Ar = 434$; (b) and (d) $Ar = 17455$. The cylinder is the same (with $l / d_o = 5.00$ and $d_i / d_o = 0.85$), the difference in Ar is due to different viscosities.

In Figure 3 the flipping process is compared between cylinders falling though liquid mixture *m1* with the cylinders having identical length l and identical outer diameter d_o but different inner diameter d_i. Clearly the effect of an increasing d_i results in a slowing of the flipping process, not only in dimensionless time tv / d_o^2 but also in real time given that d_o and v are the same for all cases shown in Figure 3. Given our Archimedes number definition of $Ar = (\gamma - 1)(d_o^2 - d_i^2) d_o g / v^2$ an increase in d_i means a decrease in Ar. Therefore, what we observe in Figure 3 can be interpreted as an increase in flipping time with a decrease in Archimedes number which fits with the trend observed in our previous study on solid cylinders [17].

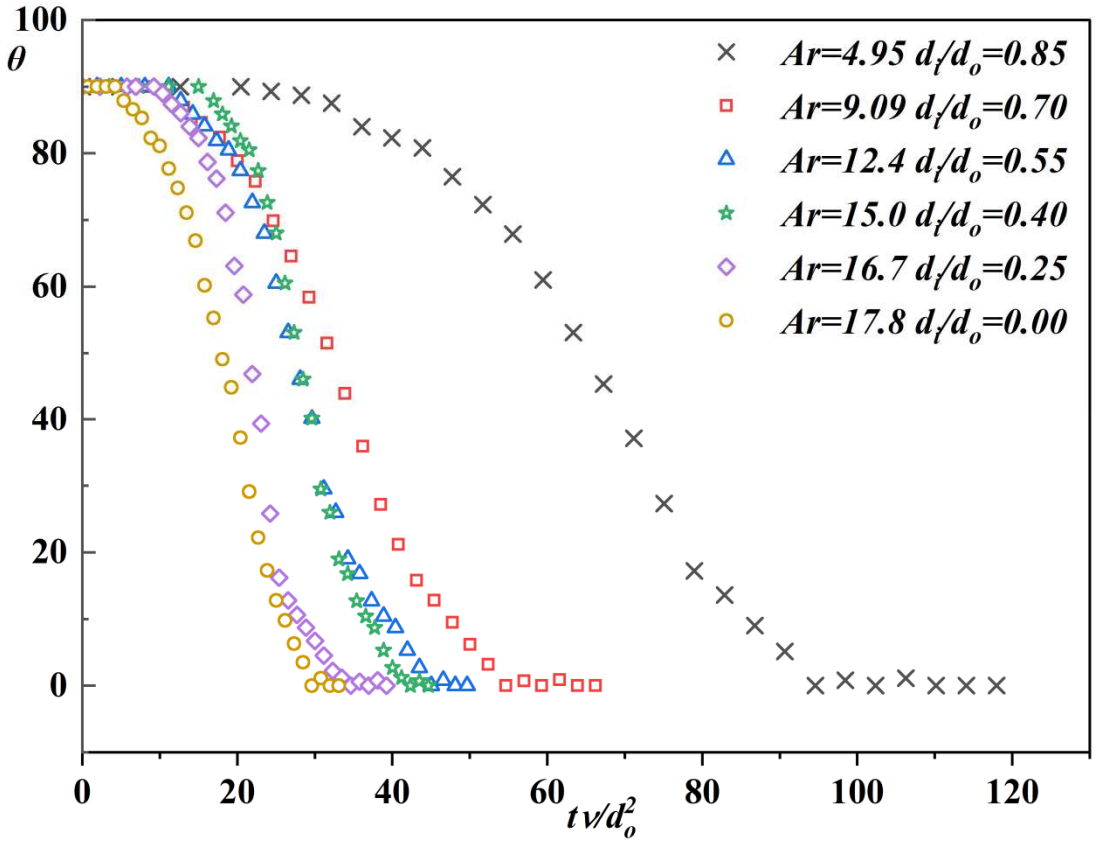

Figure 3. Time series of the angle θ of the cylinder with the horizontal plane for various d_i / d_o at $l / d_o = 5.00$. The variation of the Archimedes number is due to the variation of d_i / d_o.

Figure 4 and 5 show the vertical-to-horizontal flipping process as represented by the simulations, including checks on sensitivity to numerical parameters. Figure 4 is a qualitative impression where we not only show the cylinder, but also the flow field that is generated by the cylinder falling through the liquid. The cylinder creates a very long wake behind it which is the reason we need a tall simulation domain. Figure 4a looks at the cylinder from above. One sees that the liquid inside the cylinder has a speed comparable with the speed at the outer diameter of the cylinder, i.e. the liquid inside the cylinder largely moves with the cylinder. Below we will look at the flow through the cylinder during its sedimentation in more detail. Figure 4c is an illustration of the periodic boundary conditions, in this case in the *x*-direction; looking up from the cylinder, the wake here crosses the left boundary of the flow domain ($x = 0$) to continue at the right side $x = 12.5 d_o$. At the moment shown in Figure 4d the cylinder has completed the flipping process.

Figure 5 shows time series of the orientation angle θ and $Re = |u_z| d_o / \nu$ (the Reynolds number based on the instantaneous vertical velocity of the center of mass of the cylinder) derived from the simulations. The left panels show the effect of the spatial resolution of the simulation on the behavior of the cylinder. A simulation for which d_o spans 16 lattice spacings Δ is compared with one with $d_o = 12\Delta$. Only minor differences are observed so that we conclude that a resolution of $d_o = 12\Delta$ is reasonable. In the middle two panels we compare a hollow cylinder and a solid cylinder with the same l / d_o and the same Ar. This result supports our definition of Ar, given that the two cylinders behave comparably in terms of the time scales of flipping and associated Reynolds number. It means that the behavior of a hollow cylinder is similar to that of a solid cylinder having the same Ar and l / d_o. The right panels of Figure 5 deal with the effect of the l / d_o aspect ratio. It demonstrates that – also for hollow cylinders – the dynamics of flipping is faster for shorter cylinders, whereas the eventual settling Reynolds number is more or less independent of l / d_o. The latter is because both drag and net gravity are approximately linear functions of l.

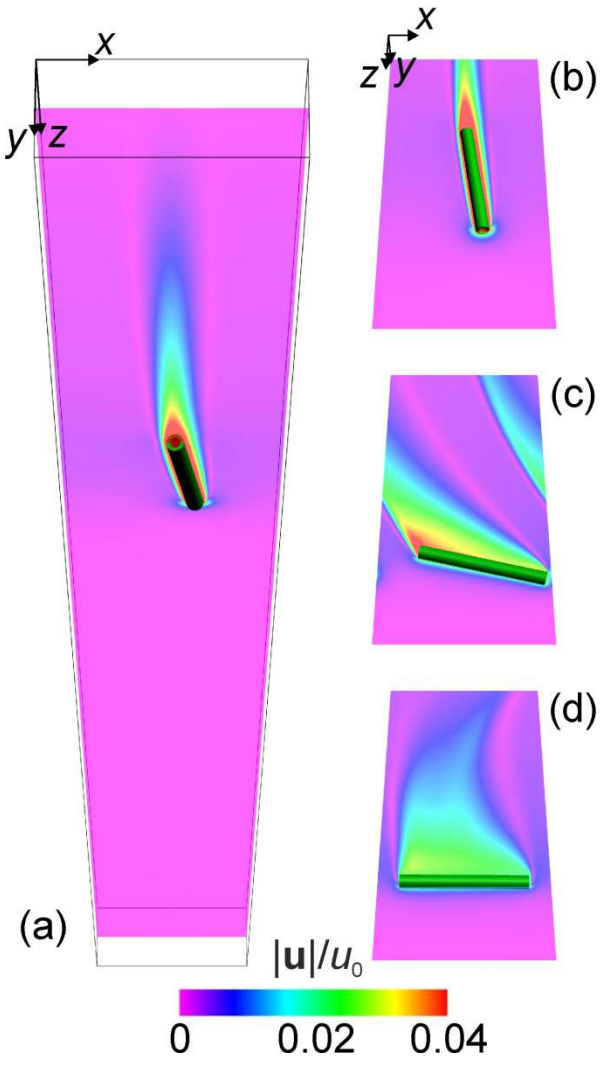

Figure 4. Impressions of a simulation at $Ar = 2057$ with $l/d_o = 9.34$ and $d_i/d_o = 0.625$. (a) Overall view of simulation domain at moment $t\nu/d_o^2 = 0.59$; (b) detailed view at the same moment; (c) and (d) detailed views at $t\nu/d_o^2 = 1.18$ and 2.36 respectively. In the color scale $u_o = (\gamma - 1)gd_o^2/\nu$.

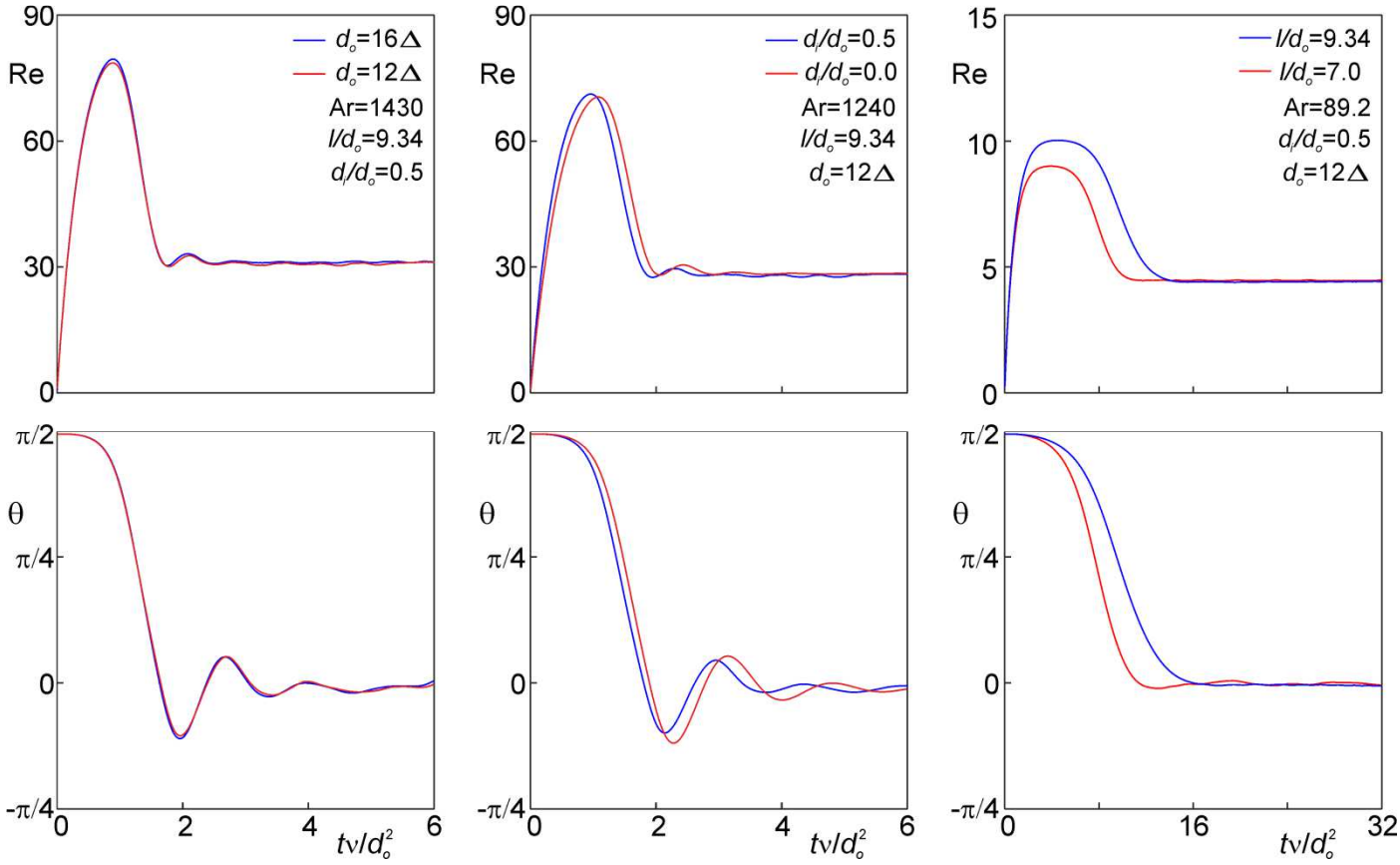

Figure 5. Simulated time series of Re (top) and θ (bottom). Left: comparison between two spatial resolutions ($d_o = 16\Delta$ and $d_o = 12\Delta$) at Ar and aspect ratios l/d_o and d_i/d_o as indicated. Middle: comparison between a hollow ($d_i/d_o = 0.5$) cylinder and a massive ($d_i/d_o = 0$) cylinder at the same Ar and l/d_o. Right: effect of l/d_o (9.34 versus 7.0) at the indicated conditions.

The simulations allow for a detailed analysis of the flow phenomena associated with the cylinder moving through liquid. Given that hollow particles are used in practical applications for enhancement of transfer processes it is worthwhile to monitor the flow rate inside a hollow cylinder. For this we have determined the average axial velocity $\langle u \rangle$ of the liquid relative to the cylinder. A sample result of how $\langle u \rangle$ is correlated with the flipping process is shown in Figure 6. Orientation and speed of the cylinder determine the strength of the flow through the cylinder. Upon vertical release the through-flow rapidly increases. After reaching a maximum value of $\langle u \rangle d_i/\nu \approx 2.8$ the through-flow gets weaker as a result of the

combined effect of rotation of the cylinder and slowing down of the cylinder. Given that Figure 6 deals with a wobbling cylinder we observe flow reversal inside the cylinder, i.e. $\langle u \rangle$ changes sign, approximately at the same moment when the cylinder becomes horizontal for the first time (at $t\nu / d_o^2 = 1.2$). We also would like to note that the Reynolds number associated with the through-flow is one to two orders of magnitude smaller than the Reynolds number associated with the settling process.

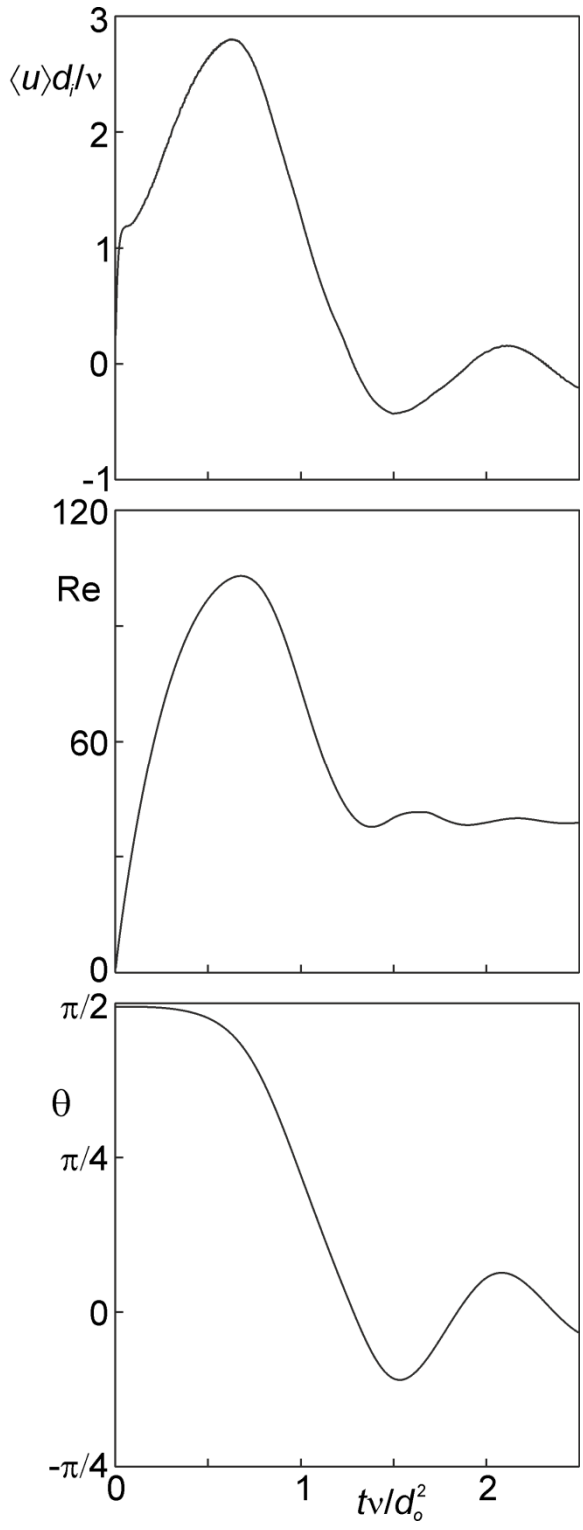

Figure 6. Top: time series of the average velocity $\langle u \rangle$ (made dimensionless by ν / d_i) of the flow through the settling cylinder. The two lower panels show how this through-flow correlates with *Re* and θ respectively. $Ar = 2057$, $l / d_o = 9.34$ and $d_i / d_o = 0.625$.

5.2 Dependencies on the Archimedes number

In this section on the effect of the Archimedes number on the settling behavior of hollow cylinders, the latter is characterized by two metrics: (1) the dimensionless time $t\nu / d_o^2$ for the cylinder to complete a 90 ° rotation; (2) the Reynolds number at that moment. Results for $t\nu / d_o^2$ are in Figure 7. The four panels we show there are for different l / d_o aspect ratios as indicated in the figure. The overall trend is clear: the cylinder flips faster with increasing Ar. For $Ar > 10$, the slope in the panels of Figure 7 is approximately -0.6 so that – given the double-logarithmic scales – $t\nu / d_o^2 \propto Ar^{-0.6}$. Data points that have different d_i / d_o are on the same trend line. This then means that with our definition of the Archimedes number as $Ar = (\gamma - 1)(d_o^2 - d_i^2) d_o g / \nu^2$ we are able to capture the flipping behavior for hollow and solid cylinders alike, i.e. our Archimedes number definition encompasses the effect d_i / d_o has. If we write the trend lines as $t\nu / d_o^2 \propto \chi Ar^{-0.6}$ the pre-factor χ depends on l / d_o. Fitting the experimental data points for $Ar > 10$ gives values of χ of 44, 57, 100 and 132 for l / d_o 2.50, 5.00, 7.50 and 10.0 respectively. This shows, as expected, an increased flipping time for longer cylinders.

Figure 7 also shows simulation data (only for $l / d_o \approx 7.5$ and 10). For $Ar > 100$ simulation results and experiments agree well. For smaller Ar, the flipping time is overestimated by the simulations. This might be due to the limits we have to put – for computational reasons – on the simulation domain size. These limits are mostly felt for low Ar as then the presence of the cylinder is felt over a larger volume of fluid surrounding the cylinder.

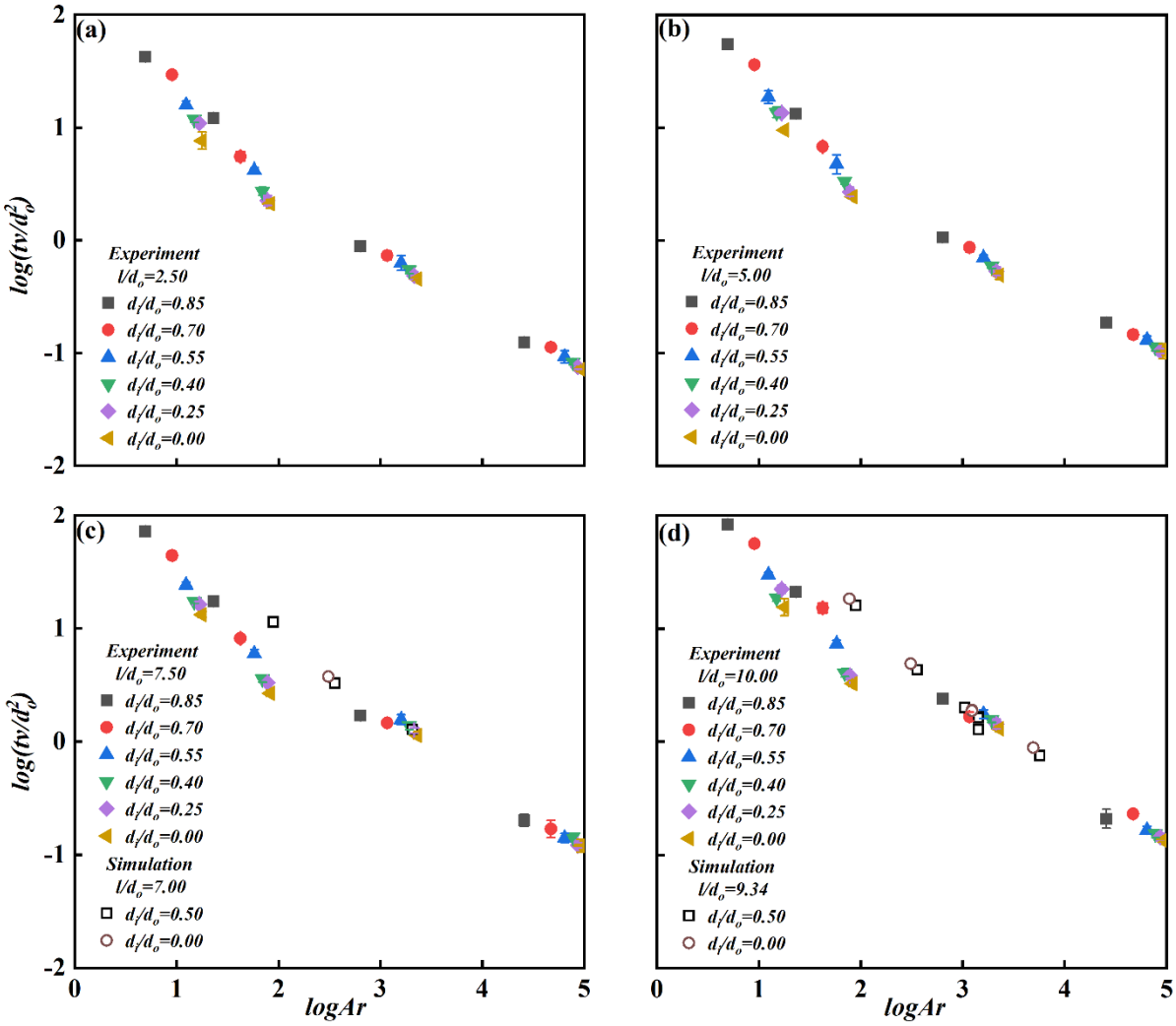

Figure 7. Dimensionless time to reaching a horizontal orientation for the first time (tv/d_o^2) versus Ar for four different l/d_o ratios (2.50, 5.00, 7.50 and 10.0 in panels (a) to (d) respectively). Variations of the Archimedes number are due to variations in viscosity as well as in d_i/d_o.

Figure 8 shows the Reynolds number based on the vertical velocity of the center of mass of the cylinder the moment it becomes horizontal for the first time. The data are organized in the same way as in Figure 7; four panels with each panel having a different l/d_o. As in Figure 7, the experimental data points in Figure 8 for different values of d_i/d_o fall approximately on the same trend line, again supporting our Ar definition. It also is observed that the Reynolds numbers are hardly sensitive to l/d_o. This we understand given that for a horizontal cylinder the drag force on a cylinder to a good approximation is proportional to its length. With net gravity also proportional to length this leads to a settling speed not (strongly)

dependent on the cylinder's length. The simulation results in terms of Reynolds number are in good agreement with experimental data.

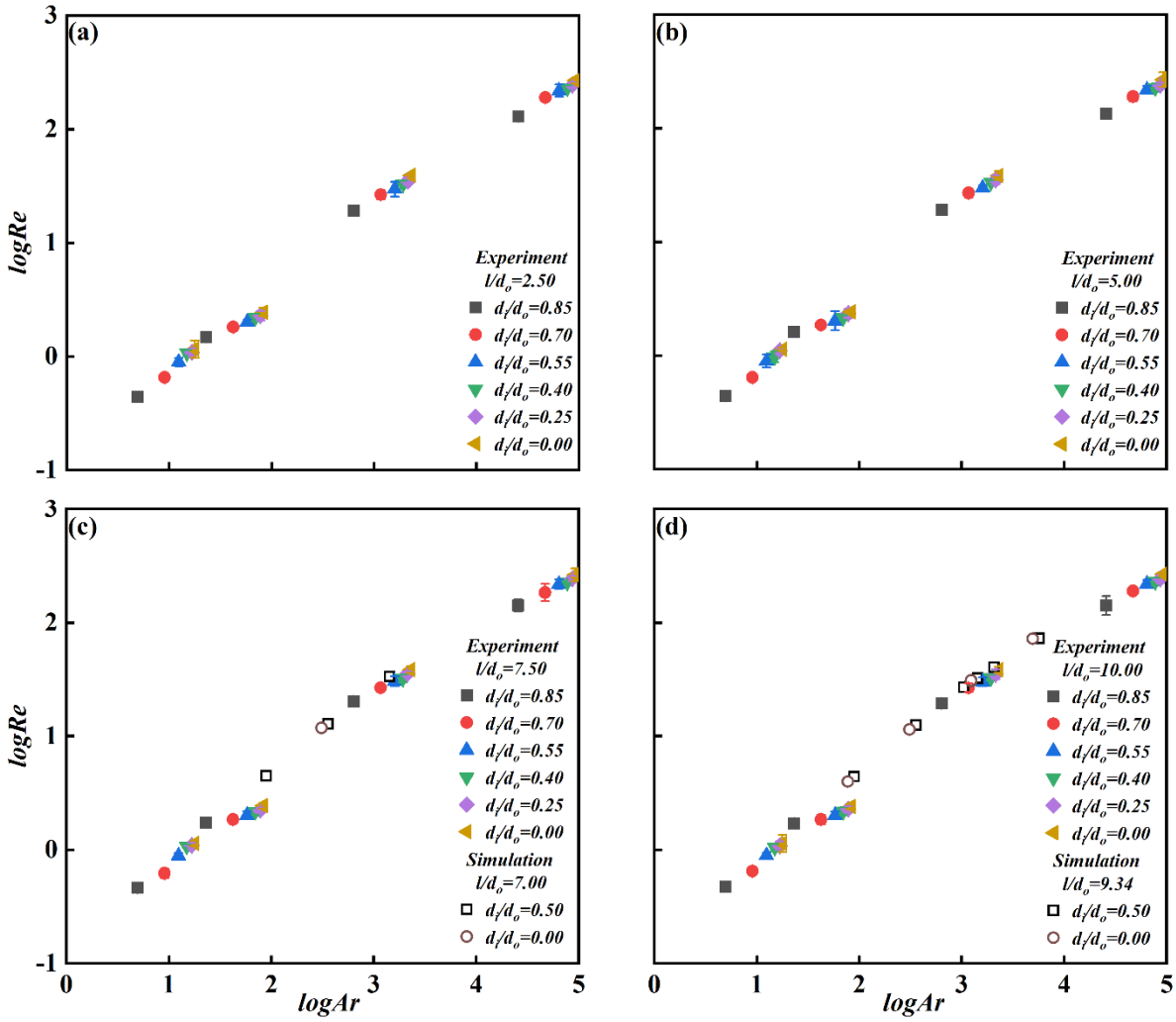

Figure 8. Reynolds number at the moment of reaching a horizontal orientation for the first time versus Ar for four different l/d_o ratios (2.50, 5.00, 7.50 and 10.0 in panels (a) to (d) respectively). Variations of the Archimedes number are due to variations in viscosity as well as in d_i/d_o.

6 Conclusion

This paper reports on settling of hollow cylinders in a Newtonian liquid. The emphasis of the work is on quantitative visualization experiments; the work is supported by particle-resolved numerical simulations. A central hypothesis of the paper is that it is feasible to correlate the behavior of solid and hollow cylinders with a single Ar, the expression of which incorporates the outer diameter and inner diameter (zero for solid cylinders). The metrics used for characterizing the sedimentation process are the time it

takes for a vertically released cylinder to reach a horizontal orientation for the first time, and the Reynolds number at that moment. The proposed expression for the Archimedes number reads $Ar = (\gamma - 1)(d_o^2 - d_i^2) d_o g / \nu^2$; it has been argued that Archimedes number is proportional to the Reynolds number based on the settling speed of a horizontal cylinder.

The experimental data show that the Reynolds number at the moment the cylinder becomes horizontal for the first time is indeed to a good approximation uniquely dependent on Ar, i.e. it hardly depends on the length over diameter aspect ratio l / d_o or on the diameter ratio d_i / d_o. The dimensionless time to horizontal orientation $t\nu / d_o^2$ depends on Ar and l / d_o, hardly on d_i / d_o.

The numerical simulations as described in this paper serve a few purposes. In the first place they provide more detail of the flow in the wake of the settling cylinder. In the second place they allow for more rigorous tests of the above-mentioned hypothesis by comparing results for cylinders with different d_i / d_o having exactly the same Ar and l / d_o. Settling of those cylinders closely match. In the third place and given that the simulations fully represent the cylinder geometry, the simulations allow for assessing the flow through the hollow cylinder during sedimentation. It is observed that the Reynolds number of the through flow is one to two orders of magnitude smaller than that of the external flow. Computational limitations mean that we cannot simulate the entire experimental flow domain. In comparing experimental and simulation results, domain size effects particularly show for the smaller Ar values where the simulations tend to overestimate the dimensionless time for rotation to horizontal.

Supporting Information

Supporting Information for this article can be found under [Link provided by Wiley].

Acknowledgment

This work was supported by the National Natural Science Foundation of China (grant numbers: 22078191, 21978165, 22081340412 and 92156020).

Symbols used

Greek letters

γ	[–]	Solid over liquid density ratio
Δ	[–]	Lattice spacing
Δt	[s]	Time step
Δz	[m]	Vertical distance between the end points
δ	[mm]	Pixel square size
δs	[m]	Vertical distance traveled by the cylinder's centre of mass
δt	[s]	Time required to shift by the cylinder's centre of mass
θ	[–]	Angle between cylinder and the horizontal plane
μ	[mPa·s]	Dynamic viscosity
ν	[m^2/s]	Kinematic viscosity
σ	[–]	Standard deviation
ρ	[g/cm^3]	Density
χ	[–]	Pre-factor

Roman letters

d	[mm]	Diameter
f	[s^{-1}]	Frame rate
g	[m/s^2]	Gravitational acceleration
l	[mm]	Length
$nx \cdot ny \cdot nz$	[mm]	Default domain size in the three Cartesian coordinate directions
t	[s]	Time
u	[m/s]	Velocity
$\langle u \rangle$	[m/s]	Average axial velocity in the cylinder

$\lvert U \rvert$	[m/s]	

Absolute value of the vertical velocity of the of the cylinder at that moment it gets horizontal

Sub- and Superscripts

h	[–]	Horizontal
i	[–]	Inner
l	[–]	Liquid
m	[–]	Dimensionless
o	[–]	Outer
s	[–]	Solid
z	[–]	Vertical

Abbreviations

Ar	[–]	Archimedes number
IB	[–]	Immersed boundary
LB	[–]	Lattice-Boltzmann
PRS’s	[–]	Particle-resolved simulations
Re	[–]	

Reynolds number when the cylinder reaches a horizontal orientation for the first time

References

[1] L. de Wit, C. van Rhee, A. Talmon, Influence of important near field processes on the source term of suspended sediments from a dredging plume caused by a trailing suction hopper dredger: the effect of dredging speed, propeller, overflow location and pulsing, *Environ. Fluid Mech.* **2015**, *15 (1)*, 41–66. DOI: 10.1007/s10652-014-9357-0

[2] G. Fromant, D. Hurther, J. van der Zanden, D. A. van der A, I. Caceres, T. O'Donoghue, J. S. Ribberink, Wave Boundary Layer Hydrodynamics and Sheet Flow Properties Under Large-Scale Plunging-Type Breaking Waves, *J. Geophys. Res. C: Oceans* **2019**, *124 (1)*, 75–98. DOI: 10.1029/2018jc014406

[3] N. G. Deen, M. van Sint Annaland, J. A. M. Kuipers, Multi-scale modeling of dispersed gas–liquid two-phase flow, *Chem. Eng. Sci.* **2004**, *59 (8-9)*, 1853–1861. DOI: 10.1016/j.ces.2004.01.038

[4] L. Q. Lu, J. Yu, X. Gao, Y. P. Xu, M. Shahnam, W. A. Rogers, Experimental and numerical investigation of sands and Geldart A biomass co-fluidization, *AlChE J.* **2020**, *66 (6)*, 1–10. DOI: 10.1002/aic.16969

[5] D. Alfonso, C. Perpiñá, A. Pérez-Navarro, E. Peñalvo, C. Vargas, R. Cárdenas, Methodology for optimization of distributed biomass resources evaluation, management and final energy use, *Biomass Bioenergy* **2009**, *33 (8)*, 1070–1079. DOI: 10.1016/j.biombioe.2009.04.002

[6] X. K. Lu, A. Bertei, D. P. Finegan, C. Tan, S. R. Daemi, J. S. Weaving, K. B. O'Regan, T. M. M. Heenan, G. Hinds, E. Kendrick, D. J. L. Brett, P. R. Shearing, 3D microstructure design of lithium-ion battery electrodes assisted by X-ray nano-computed tomography and modelling, *Nat. Commun.* **2020**, *11 (1)*, 2079. DOI: 10.1038/s41467-020-15811-x

[7] A. Andersson, J. Holmberg, R. Haggblad, Process Improvements in Methanol Oxidation to Formaldehyde: Application and Catalyst Development, *Top. Catal.* **2016**, *59 (17-18)*, 1589–1599. DOI: 10.1007/s11244-016-0680-1

[8] B. Partopour, A. G. Dixon, Effect of particle shape on methanol partial oxidation in a fixed bed using CFD reactor modeling, *AlChE J.* **2020**, *66 (5)*, 1–13. DOI: 10.1002/aic.16904

[9] S. Movahedirad, A. M. Dehkordi, E. A. Molaei, M. Haghi, M. Banaei, J. A. M. Kuipers, Bubble Splitting in a Pseudo-2D Gas-Solid Fluidized Bed for Geldart B-Type Particles, *Chem. Eng. Technol.* **2014**, *37 (12)*, 2096–2102. DOI: 10.1002/ceat.201300565

[10] G. E. Stringham, D. B. Simons, H. P. Guy, The Behavior of Large Particles Falling in Quiescent Liquids, *U.S. Geol. Surv. Prof. Pap. U.S.* **1969**.

[11] P. D. Komar, C. Reimers, Grain Shape Effects on Settling Rates, *J.Geol.* **1978**, *86 (2)*, 193–209. DOI: 10.1086/628496

[12] C. Toupoint, P. Ern, V. Roig, Kinematics and wake of freely falling cylinders at moderate Reynolds numbers, *J. Fluid Mech.* **2019**, *866*, 82–111. DOI: 10.1017/jfm.2019.77

[13] Z. H. Cheng, A. Wachs, An immersed boundary/multi-relaxation time lattice Boltzmann method on adaptive octree grids for the particle-resolved simulation of particle-laden flows, *J. Comput. Phys.* **2022**, *471*, 111669. DOI: 10.1016/j.jcp.2022.111669

[14] M. Uhlmann, Interface-resolved DNS of vertical particulate channel flow in the turbulent regime, *Phys. Fluids* **2008**, *20 (5)*, 053305. DOI: 10.1063/1.2912459

[15] A. Wachs, L. Girolami, G. Vinay, G. Ferrer, Grains3D, a flexible DEM approach for particles of arbitrary convex shape — Part I: Numerical model and validations, *Powder Technol.* **2012**, *224*, 374–389. DOI: 10.1016/j.powtec.2012.03.023

[16] J. J. Derksen, Settling and fluidization of tall cylinders in solid-liquid suspensions, *AlChE J.* **2023**, *e18072*. DOI: 10.1002/aic.18072

[17] J. H. Xie, L. J. Zhang, M. H. Lu, J. Lu, J. J. Derksen, Experiments and simulations of settling cylinders over a wide range of Archimedes numbers, *Can J Chem Eng* **2022**, *101(4)*, 2240–2249. DOI: 10.1002/cjce.24544

[18] S. Succi, The Lattice Boltzmann Equation for Fluid Dynamics and Beyond, *Oxford University Press, Oxford* **2002**. DOI: 10.1063/1.1537916
[19] H. M. Kushwaha, S. K. Sahu, Effects of Viscous Dissipation and Rarefaction on Parallel Plates with Constant Heat Flux Boundary Conditions, *Chem. Eng. Technol.* **2015**, *38 (2)*, 235–245. DOI: 10.1002/ceat.201400264
[20] T. Kruger, H. Kusumaatmaja, A. Kuzmin, O. Shardt, G. Silva, E. M. Viggen, The Lattice Boltzmann Method Principles and Practice, *Springer International Publishing AG Switzerland* **2017**. DOI: 10.1007/978-3-319-44649-3
[21] M. Uhlmann, An Immersed Boundary Method with Direct Forcing for the Simulation of Particulate Flows, *J. Comput. Phys.* **2005**, *209 (2)*, 448–476. DOI: 10.1016/j.jcp.2005.03.017
[22] A. t. Cate, C. H. Nieuwstad, J. J. Derksen, H. E. A. V. d. Akker, Particle imaging velocimetry experiments and lattice-Boltzmann simulations on a single sphere settling under gravity, *Phys. Fluids* **2002**, *14 (11)*, 4012–4025. DOI: 10.1063/1.1512918
[23] J. B. Kuipers, Quaternions and rotation sequences: a primer with applications to orbits, aerospace, and virtual reality, *Aeronaut. J.* **1999**, *103 (1021)*, 127–143. DOI: 10.1017/S0001924000065039

Table and Figure captions

Table S1. Density and viscosity at 25 ± 1 □ for the various liquid mixtures used in the experiments

Mixture id	Density ρ_s (g/cm^3)	Standard deviation $\sigma(\rho_l)$ (g/cm^3)	Dynamic viscosity μ (mPa·s)	Standard deviation $\sigma(\mu)$ (mPa·s)	Kinematic viscosity ν (10^6 m^2/s)
m1	1.238	0.0094	191	8.0	154.3
m2	1.234	0.0158	178	6.8	144.2
m3	1.230	0.0266	160	5.2	130.3
m4	1.211	0.0133	99	2.3	81.8
m5	1.204	0.0083	80	1.5	66.4
m6	1.192	0.0887	64	0.83	53.7
m7	1.142	0.1223	16	0.28	14.4
m8	1.103	0.0403	6.4	0.025	5.8
m9	1.051	0.0541	2.5	0.013	2.4

Figure 1. (a) Sample camera frames of a settling experiment recorded at 100 Fps for a $d_i / d_o = 0.85$ and $l / d_o = 5.00$ hollow cylinder falling through a glycerol-water mixture ($Ar = 4.95$). (b) Time series of the angle θ of the hollow cylinder with the horizontal plane.

Figure 2. Impressions of the flipping process and the way it depends on Ar. Image frames and corresponding θ time series. (a) and (c) have $Ar = 434$; (b) and (d) $Ar = 17455$. The cylinder is the same (with $l / d_o = 5.00$ and $d_i / d_o = 0.85$), the difference in Ar is due to different viscosities.

Figure 3. Time series of the angle θ of the cylinder with the horizontal plane for various d_i / d_o at $l / d_o = 5.00$. The variation of the Archimedes number is due to the variation of d_i / d_o.

Figure 4. Impressions of a simulation at $Ar = 2057$ with $l/d_o = 9.34$ and $d_i/d_o = 0.625$. (a) Overall view of simulation domain at moment $t\nu/d_o^2 = 0.59$; (b) detailed view at the same moment; (c) and (d) detailed views at $t\nu/d_o^2 = 1.18$ and 2.36 respectively. In the color scale $u_o = (\gamma - 1)gd_o^2/\nu$.

Figure 5. Simulated time series of *Re* (top) and θ (bottom). Left: comparison between two spatial resolutions ($d_o = 16\Delta$ and $d_o = 12\Delta$) at *Ar* and aspect ratios l/d_o and d_i/d_o as indicated. Middle: comparison between a hollow ($d_i/d_o = 0.5$) cylinder and a massive ($d_i/d_o = 0$) cylinder at the same *Ar* and l/d_o. Right: effect of l/d_o (9.34 versus 7.0) at the indicated conditions.

Figure 6. Top: time series of the average velocity $\langle u \rangle$ (made dimensionless by ν/d_i) of the flow through the settling cylinder. The two lower panels show how this through-flow correlates with *Re* and θ respectively. $Ar = 2057$, $l/d_o = 9.34$ and $d_i/d_o = 0.625$.

Figure 7. Dimensionless time to reaching a horizontal orientation for the first time ($t\nu/d_o^2$) versus *Ar* for four different l/d_o ratios (2.50, 5.00, 7.50 and 10.0 in panels (a) to (d) respectively). Variations of the Archimedes number are due to variations in viscosity as well as in d_i/d_o.

Figure 8. Reynolds number at the moment of reaching a horizontal orientation for the first time versus *Ar* for four different l/d_o ratios (2.50, 5.00, 7.50 and 10.0 in panels (a) to (d) respectively). Variations of the Archimedes number are due to variations in viscosity as well as in d_i/d_o.

Highlights

- Quantitative visualization experiment of the settlement of a single hollow cylinder.
- The flipping process under different Archimedes numbers is studied.
- The effect of aspect ratio and Archimedes numbers on the dimensionless time and the Reynolds number are studied.
- Numerical simulation was used to verify the experimental data.